ROYAL SOCIETY
OF CHEMISTRY

PAPER

Check for updates

Optical properties of extreme tellurium nanowires formed in subnanometer-diameter channels

Vladimir V. Poborchii, [ID] *[ab] Alexander V. Fokin[a] and Alexander A. Shklyaev[cd]

Single tellurium (Te) chains attract much attention as extreme nanowires with unique electronic and spintronic properties. Here, we encapsulate Te from a melt into channels of zeolites AFI ($\sim$0.73 nm-channel diameter) and mordenite (MOR, $\sim$0.67 $\times$ 0.7 nm^2 channel cross-section) *via* high-pressure injection. Using polarized Raman and optical absorption spectra (RS and OAS) of zeolite single crystals with Te (AFI-Te and MOR-Te), we discriminate between features of Te chains and rings formed in the zeolites. We demonstrate good agreement of AFI-Te-chain RS and OAS with the calculated single Te-helix phonon and electron spectra. This suggests a very weak interaction of the AFI-Te-chain with the zeolite and its nearly perfect helix structure lacking inversion/mirror symmetry. An AFI-Te OAS feature, attributed to the electron transitions between Te-helix-Rashba-split valence and conduction bands confirms its 1D-electron-band origin with predicted possibilities of identifying Majorana fermions, manipulating spin transport and realizing topological superconductivity.

Introduction

Bulk trigonal Te (t-Te) consists of parallel interacting helical chains of atoms (Fig. 1(a)). Interchain bonds are partially van der Waals (vdW) and partially covalent due to an overlap of lone-pair electron orbitals with anti-bonding states of adjacent chains. Extreme 1D nanowires (NWs), such as isolated single Te chains, displaying only vdW interaction with the environment and a pure 1D-electron-band structure, are expected to show unique electronic properties completely different from those of bulk Te. This attracts much attention to the single Te chain fabrication and its properties. Encapsulation of Te in carbon nanotubes was recently reported.[1–3] Other techniques including exfoliation[4] were also used towards obtaining single Te chains. Te NWs are considered as successors of silicon for extremely scaled semiconductor devices.[5] Te NWs encapsulated in boron nitride nanotubes exhibited an extremely high current density of 1.5 $\times$ 10^8 A cm^{-2}.[2] But this was not a single Te chain NW property. Fabrication and reliable characterization of single Te chains with the predicted giant Rashba spin splitting (which implies a possibility of identifying Majorana fermions, manipulating spin transport, and realizing topological superconductivity),[6] is still a challenge. Here, we fabricate single Te chains in subnanometer-diameter channels of zeolites AFI and mordenite

(MOR) and study their phonon and electron spectra. We show that the phonon/electron spectra of the AFI-confined Te chains are close to those of the perfect 1D Te helix, which is, in fact, the first ever experimental study of such properties.

About 50 years ago, single Se/Te chains attracted attention as building units of amorphous Se/Te (a-Se, a-Te).[7–10] It was shown that a-Se/Te mainly consists of weakly interacting (*via* nearly pure vdW forces) disordered chains, intrachain bonds being strengthened compared to those in t-Se/Te at the expense of the interchain ones. Accordingly, the Te chain vibrational bond-stretching symmetric mode (BSSM) frequency in a-Te ($\sim$ 157 cm^{-1}) is higher than that in t-Te ($\sim$ 122 cm^{-1}).[7,9]

Single Se/Te chains were experimentally studied from the early 1980s when Se/Te was encapsulated in MOR channels with $\sim$0.67 $\times$ 0.7 nm^2 cross-sections. Optical absorption spectral (OAS) anisotropy with a strong absorption for the light polarized along channels due to the formed Se/Te chains was observed for MOR with Se (MOR-Se) and MOR with Te (MOR-Te).[11,12] The intrachain bond enhancement in the isolated Se/Te chains, compared to those in t-Se and t-Te, was demonstrated *via* Raman Spectra (RS) of MOR-Se/Te showing the increase of BSSM frequencies in single chains.[13,14] Later, MOR-Se X-ray absorption and electron-microscopy studies were performed.[15–17]

Se/Te chains were considered as the sole species formed in MOR channels until the polarized RS of MOR-S/Se/Te single crystals suggested that the S/Se/Te chains coexist with S/Se/Te rings, respectively.[18] Further studies of Se species confined in the channels of MOR and another zeolite AFI with $\sim$0.73 nm diameter confirmed the formation of chains and rings discriminated *via* polarized RS/OAS of MOR-Se and AFI-Se single crystals.[19–23]

[a]Ioffe Physico-Technical Institute, St. Petersburg 194021, Russia. E-mail: vladimir. poborchii@gmail.com

[b]National Institute of Advanced Industrial Science and Technology, Tsukuba 305-8565, Japan

[c]Novosibirsk State University, 2 Pirogov Str., Novosibirsk 630090, Russia

[d]Rzhanov Institute of Semiconductor Physics SB RAS, 13 Lavrentiev Aven., Novosibirsk 630090, Russia
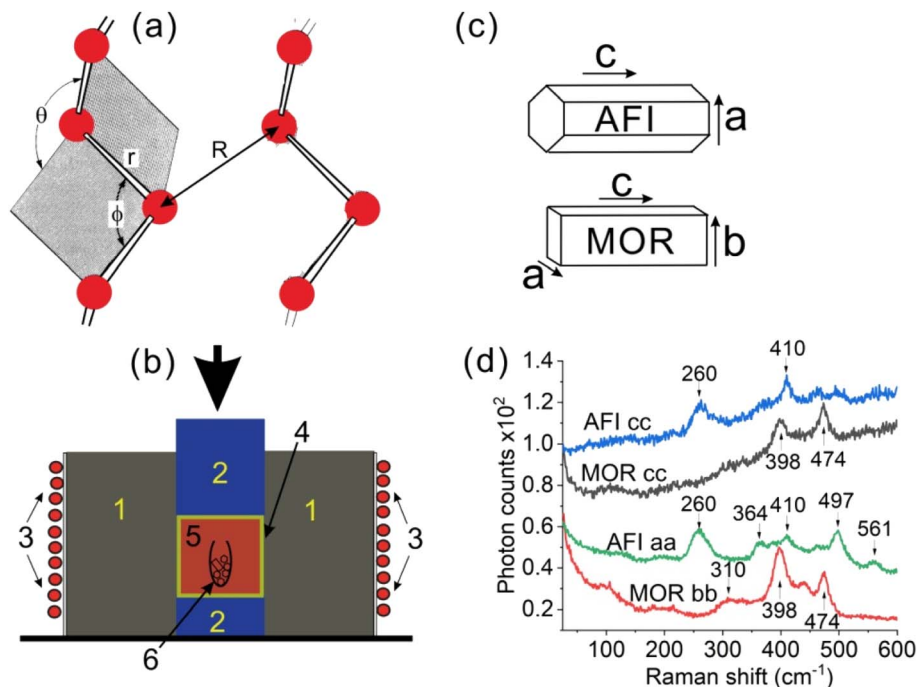
Fig. 1 (a) t-Te crystal structure: intrachain bond length $r = 0.2835$ nm, interchain bond length $R = 0.3495$ nm, bond angle $\phi = 103.2°$ and dihedral angle $\theta = 100.7°$ taken from ref. 9; (b) a cross-section of the high-pressure (the big arrow on the top shows its direction) melt injection system with a steel chamber – 1, pistons – 2, a wire heater – 3, a stainless steel ampoule – 4, molten tellurium – 5, and a quartz ampoule with zeolites – 6; (c) AFI and MOR crystal shapes: a hexagonal prism with a length up to 150 μm and a rectangular prism with a length up to 400 μm, respectively; (d) Raman spectra of bare AFI and MOR zeolites excited with a 514.5 nm wavelength laser.

Returning to the recent results on the high-resolution-electron-microscopy (HREM) observation of the CNT-confined Te chains, we should note that the HREM images of the Te helical chains in CNTs with diameters $d = 0.86–0.96$ nm [1] look convincing while the images of Te structures in the smallest CNTs with $d \sim 0.75$ nm [1] and $d \sim 0.83$ nm [2] are rather confusing. Anyway, despite the huge interest in single Te helix properties, there is a lack of experimental results in this matter.

Here, we encapsulate tellurium in channels of AFI via high-pressure-Te-melt injection, for the first time, and show evidence that single-helical-Te-chain formation is achieved. We show that the AFI-Te chains display polarized RS/OAS consistent with theoretical phonon/electron spectra predicted for the single Te helix. We compare AFI-Te chain results with those of MOR-Te chains re-examined via much better equipment than in early studies.[14,18] We conclude that the AFI-Te chains are ordered and weakly interacting with the zeolite while MOR-Te chains are, probably, shorter, less ordered and strongly interacting with the zeolite. We conclude that nearly pure 1D phonon and electron band structures are experimentally realized in the AFI-Te chains.

Experimental methods

Te was introduced into zeolites from a melt under ~ 20 kbar pressure using the method described in ref. 24 (Fig. 1(b)). Synthetic AFI ($Al_{12}P_{12}O_{48}$), that is pure $AlPO_4$-5, and natural MOR ($Ca_2Na_4Si_{40}Al_8O_{96}$) the same as in ref. 23 were used (Fig. 1(c)). The zeolite structures are accessible in ref. 25 and 26. AFI was first calcined at a temperature of ~ 550 °C then both AFI

and MOR were dehydrated at ~ 500 °C before the Te encapsulation. Fig. 1(b) schematically illustrates the technique of the molten Te injection into zeolites. The device consists of a cylindrical steel chamber with an encircling wire heater. Zeolites were placed into a quartz ampoule inside a stainless-steel ampoule with molten Te. The pressure was applied via steel pistons on the stainless-steel ampoule with the Te melt at a temperature of ~ 500 °C.

We should note that the utilization of the high-pressure melt injection instead of Te vapour adsorption is crucial in the case of AFI-Te since a number of experiments showed that AFI is a weak adsorber of Te vapour although MOR is a rather effective one.[27,28] According to ref. 28, AFI containing no Si atoms in its framework, like in our case, shows zero adsorption ability for Te while AFI with the formula $Al_{11.8}Si_{1.1}P_{11.1}O_{48}$ was able to adsorb ~ 0.3 Te atoms per AFI unit cell, which is about one order lower than the Te loading density achieved by the high-pressure melt injection. Electron-probe micro-analysis suggests loading densities of ~ 3.5 and ~ 4.5 Te atoms per unit cell for AFI-Te and MOR-Te, respectively. Since the MOR unit cell contains two large channels while the AFI unit cell possesses only one channel, AFI has more Te atoms per channel than MOR has. Taking into account the AFI/MOR unit cell size of $\sim 8.5/7.5$ nm along the channels, we obtain the Te loading densities of $\sim 4/\sim 3$ atoms per nm of channel.

Raman measurements of zeolites with Te were done in air at room temperature using a Renishaw micro-Raman spectrometer equipped with a 785 nm wavelength laser. A few additional experiments were performed using a Nanofinder-30 Raman/AFM

system equipped with a 561 nm wavelength laser. The laser beams with a power of <0.1 mW were focused on an ~1 μm-diameter spot. RS of the initial AFI and MOR (Fig. 1(d)) were recorded using a JASCO micro-spectrometer with ~100 mW-power-514.5 nm-wavelength excitation.

OAS in the near-IR and visible and spectral ranges were recorded using an Ocean-Optics micro-spectrometer with optical fibers allowing to probe ~5 μm areas of samples. To avoid zeolite-surface light scattering and improve transmittance, samples were immersed in glycerol. Single-crystal zeolite samples were intentionally broken into pieces of few-micron or submicron thickness reducing optical density.

AFI–Te Raman spectra: Te helical chain and Te$_8$ ring formation

Fig. 2(a) shows the AFI structure cross-section perpendicular to its c-axis with ~0.73 nm-diameter channels. Fig. 2(b) demonstrates Te-chain-induced AFI-Te optical-absorption anisotropy *via* the light-transmittance photo-images taken for the light-polarization parallel to the AFI c-axis ($E//c$) and perpendicular to it ($E//a$), bare AFI being transparent. Fig. 2(c) reproduces calculated phonon dispersion curves for a single Te helix[1] while Fig. 2(d) shows our experimental AFI-Te RS for cc- and aa-polarization configurations (where the first/second indices stand for the polarization of the incident/scattered light). The measurement was done with an excitation wavelength of $\lambda = 785$ nm. The dominant Te-chain band is clearly displayed in the cc-configuration spectrum at ~176 cm^{-1}. The band disappears when the polarization configuration is changed to aa, with only the Te-ring band remaining at ~184 cm^{-1} in the bond-stretching-mode range of the spectrum. Importantly, the initial AFI RS display no strong bands in this spectral range even when excited with much higher laser power (Fig. 1(d)).

The ~176 cm^{-1} AFI-Te-chain frequency is in good agreement with the calculated frequencies of the upper (green and blue) bond-stretching-phonon branches of the Te helix[1] (Fig. 2(c)) as well as with other results.[29] The observed frequency of single AFI-Te chains is much higher than ~122 cm^{-1} of the interacting Te chains in t-Te.[9] We admit that the AFI-Te-chain RS selection rule is slightly relaxed and, in fact, both green and blue branches contribute to the observed ~176 cm^{-1} band. The ~184 cm^{-1} shoulder in the AFI-Te cc-spectrum belongs to Te$_8$ rings as we explain below.

The ~15 cm^{-1} experimental band (Fig. 2(d)) can be attributed to the X-point-torsional modes; the ~37 cm^{-1} band can be assigned to the X-point-bending modes (violet curve); and the ~61 cm^{-1} band can originate from the upper branches of bending modes. The slight 1st-order Raman activity of X-point-phonons confirms some wave-vector-selection-rule relaxation.
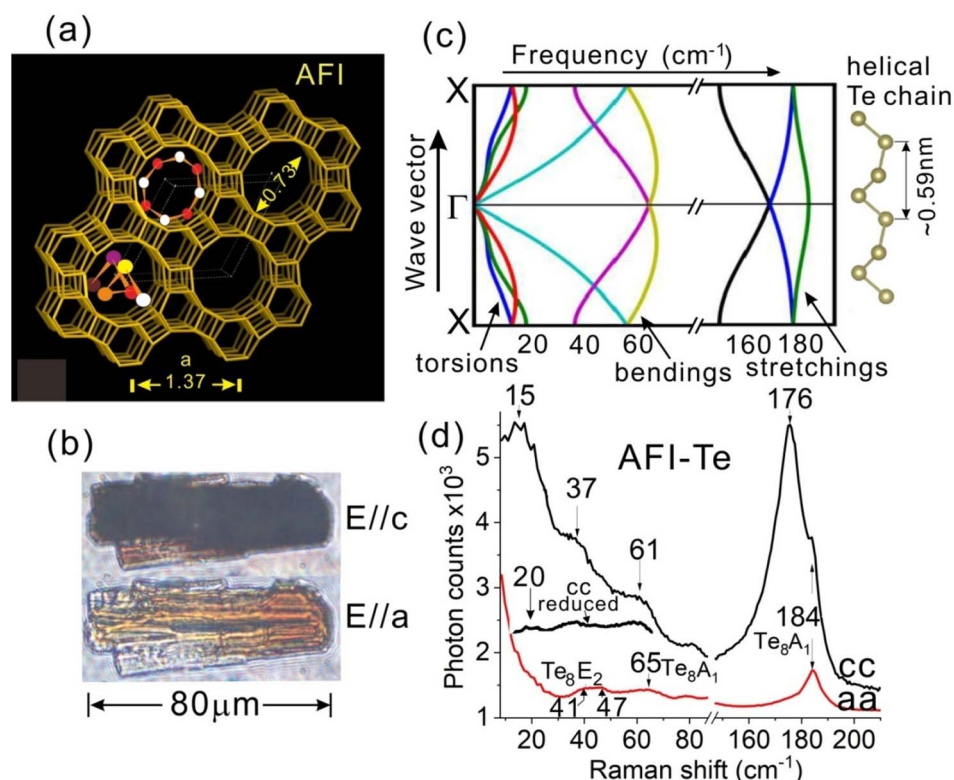
Fig. 2 (a) AFI cross-section with a trigonal helical Te chain and Te$_8$ ring schematically shown, with the brighter atom colour corresponding to its closer position to the reader; (b) transmitted light photo-images of the intentionally-broken AFI-Te crystal with ~80 μm size along the c-axis for two polarizations of light $E//c$ and $E//a$; (c) calculated phonon dispersion curves of a trigonal helical Te chain schematically shown on the right;[1] (d) AFI-Te RS excited with a 785 nm laser for cc − (black) and aa − (red) polarization configurations with a low-frequency fragment of the mathematically reduced cc-spectrum.

The low-frequency background in the AFI-Te cc-spectrum looks stronger than that in the aa-spectrum. This can be associated with a continuum of Te-chain vibrational states. Since the low-frequency part of the spectrum is enhanced due to the Bose–Einstein factor, we also show a reduced cc-spectrum $I_r(\nu)$ that is obtained from the experimental one $I_e(\nu)$ using the equation $I_r(\nu) = I_e(\nu) \times (1 - \exp(-h\nu/kT))$, where ν is the frequency and T stands for the temperature while h and k are the Planck's and Boltzmann's constants, respectively. This transformation reveals that the low-frequency band is not too strong and shifted to ~ 20 cm^{-1} from its ~ 15 cm^{-1} position in the raw spectrum (Fig. 2(d)). Positions of higher frequency bands are not affected by the transformation.

The ~ 184 cm^{-1} band in the aa-spectrum of AFI-Te (Fig. 2(d)) is assigned to the Te$_8$ ring BSSM observed earlier at ~ 182 cm^{-1} in the spectra of Te confined in the 1.14 nm-diameter nearly spherical cavities of the LTA zeolite.[30] Bond-bending modes of Te$_8$, earlier observed at ~ 45 cm^{-1} (E$_2$) and ~ 62 cm^{-1} (A$_1$),[30] are also displayed in the AFI-Te aa-spectrum as a doublet at ~ 41–47 cm^{-1} and a singlet at ~ 65 cm^{-1}, respectively. Frequency enlargements from ~ 182 cm^{-1} to ~ 184 cm^{-1} and from ~ 62 cm^{-1} to ~ 65 cm^{-1} suggest some compression of Te$_8$ in AFI compared to that in the larger diameter LTA-cavity that is able to accommodate Se$_{12}$ rings[31,32] and under certain conditions even more Se atoms.[33] A significant splitting of the E$_2$ band implies a reduction of the initial D_{4d} ring symmetry.

Finalizing this section, we should note that energetically S/Se/Te chains and rings with nearly the same bond lengths, bond angles and dihedral angles are close to each other. However, in the bulk crystalline form, S rings and Te chains are the most stable, with Se being intermediate producing rings and chain crystals. In the restricted spaces of zeolite channels, both chains and rings can be formed.

MOR-Te Raman spectra with Te chains and Te$_6$ ring bands

MOR possesses two channel systems along its c-axis (Fig. 3(a)). Wide channels have an $\sim 0.67 \times 0.7$ nm^2 cross-section, while narrow channels have a cross-section of $\sim 0.26 \times 0.44$ nm^2 that are unable to accommodate any Se/Te species.[16,34]

Fig. 3(b) shows transmitted-light photo-images of MOR-Te for $E//c$ and $E//b$ which clearly demonstrate the crystal absorption anisotropy due to Te-chain formation, bare MOR being transparent. MOR-Te RS with $\lambda = 785$ nm for the cc-, aa- and bb-polarization configurations are shown in Fig. 3(c). A dominant Te-chain band is displayed at ~ 168 cm^{-1} in the cc-spectrum while it disappears in the aa- and bb-spectra. The lower frequency and larger width of the MOR-Te-chain band compared to that of AFI-Te (half-width of ~ 18 cm^{-1} $vs.$ ~ 12 cm^{-1}) suggests its stronger interaction with the zeolite, shorter length and some disorder. The reduced MOR-Te cc-spectrum, obtained via the same transformation as that of AFI-Te, reveals one more Te-chain peak at ~ 35 cm^{-1} (Fig. 3(c)) that originates from bond-bending modes.

The bands in the MOR-Te RS at ~ 67 cm^{-1}, ~ 87 cm^{-1}, ~ 164 cm^{-1} and 196 cm^{-1} should be attributed to Te$_6$ rings. All four bands are allowed by the Te$_6$ ring (D_{3d} symmetry, Fig. 3(c) inset) RS selection rules, namely: ~ 67 cm^{-1} (E$_g$) and ~ 87 cm^{-1} (A$_{1g}$) are bond-bending modes while ~ 164 cm^{-1} (E$_g$) and 196 cm^{-1} (A$_{1g}$) are bond-stretching modes. The bands are similar to the ~ 103 (E$_g$), ~ 135 (A$_{1g}$), ~ 220 (E$_g$) and ~ 274 (A$_{1g}$) cm^{-1} bands of Se$_6$.[23] The bond-stretching-mode band at ~ 164 cm^{-1} and the bond-bending-mode bands at ~ 67 cm^{-1} and ~ 87 cm^{-1} are active in the aa-configuration and suppressed in the bb-spectrum. This means that the Te$_6$ xy plane (Fig. 3(c) inset) is normal to the b-axis of MOR (Fig. 3(a)) similar to that of Se$_6$ in MOR-Se.[18,22,23] Since the Te$_6$ size in the y-direction is larger than that in the x-direction, the ring is, probably, oriented with its y-axis along the MOR channel.

Interestingly, the Te$_6$ BSSM frequency of ~ 196 cm^{-1} coincides with that observed for Te confined in CNTs with $d \sim 0.83$ nm (CNT(0.83)-Te) and is attributed to the single Te helix.[2] However, similar to MOR-Te, Te$_6$ might be placed into such CNTs. On the other hand, smaller Te molecules also could produce a band at ~ 196 cm^{-1}. For example, a BSSM frequency of ~ 195 cm^{-1} was observed for the Te$_3$ molecule stabilized in the solid-argon matrix.[35] Another candidate is the Te$_2^-$ diatomic
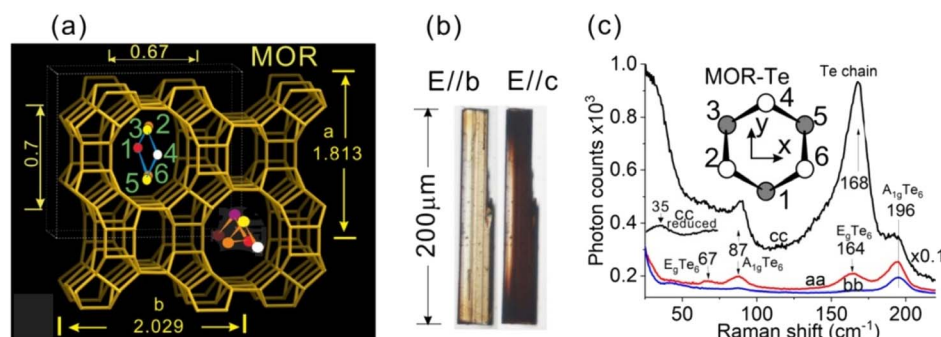

Fig. 3 (a) MOR cross-section with a trigonal helical Te chain and Te$_6$ ring schematically shown, with the brighter atom colour corresponding to its closer position to the reader; (b) transmitted-light photo-images of the MOR-Te crystal with sizes 4 μm × 20 μm × 200 μm along a-, b- and c-axes, correspondingly, for two polarizations of light $E//c$ and $E//b$; (c) Raman spectra of MOR-Te excited with a 785 nm laser for cc − (black), aa − (red) and bb − (blue) polarization configurations with a low-frequency fragment of the mathematically reduced cc-spectrum and the inset showing a Te$_6$ view along its 3-fold axis.

anion with a theoretically predicted frequency of $\sim$205 cm^{-1} that can be reduced by the environment.[36] Polarized RS of aligned CNT(0.83)-Te could clarify the origin of the $\sim$196 cm^{-1} band.

Further, the HREM image of CNT(0.75)-Te[1] is similar to that of CNT(0.83)-Te,[2] namely 1D periodic structures with separations of $\sim$0.235 nm and $\sim$0.22 nm are observed, respectively. However, in contrast to ref. 2, the authors of ref. 1 attributed the image to linear Te chains, which are rather exotic and require a negative charge on Te/Se atoms. For example, linear Te chains with -1.5 charge per atom were found in the Ba$_3$ScTe$_5$ crystals[37] and linear Se chains consisting of Se$_2^{2-}$ anions were observed in channels of cancrinite.[38–40] Anyway, it is difficult to judge about

Te-structures formed in CNT(0.75/0.83)-Te from their HREM images.[1,2] Moreover, electron-beam-induced heating might cause temperature-induced single-chain structure changes like those in AFI-Se.[41]

Te chain optical absorption and resonance Raman spectra: probing Rashba splitting

Large Rashba spin splitting is important for applications in spintronics. Recently, it was theoretically shown that a single Te helix with a Rashba parameter of $\sim$0.84 eV Å in the unstrained state and a possibility of its enhancement with strain is a good
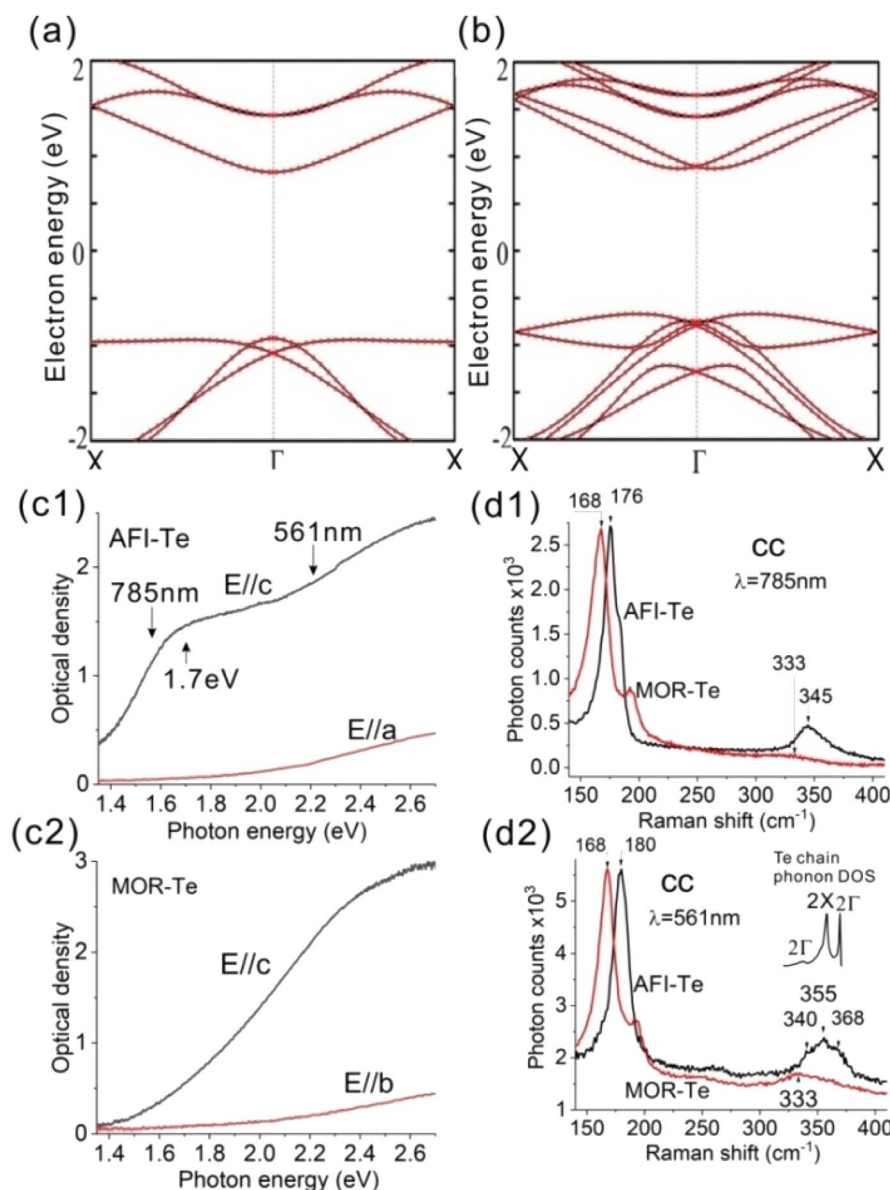
Fig. 4 (a) Calculated electron band structures of a single Te helix without (a) and with (b) spin–orbit coupling. Optical absorption spectra of AFI-Te for E//c and E//a (c1) and MOR-Te for E//c and E//b (c2); (d1) 1st- and 2nd-order Te chain Raman spectra of AFI-Te (black) and MOR-Te (red) excited with a 785 nm wavelength laser; (d2) 1st- and 2nd- order Te chain Raman spectra of AFI-Te (black) and MOR-Te (red) excited with a 561 nm wavelength laser (the inset shows the calculated Te chain phonon density of states in the doubled frequency scale).

candidate for this.[6] Fig. 4(a) and (b) show Te-helix-electron-energy bands calculated without (a) and with (b) spin–orbit coupling. In the first case, the energy band gap of $\sim$1.75 eV is organized between conduction and valence bands at the Γ-point of the BZ. In the second case, due to the Rashba splitting, electron-band minima/maxima are shifted from the Γ-point with the band-gap reduction to $\sim$1.53 eV.[6]

Fig. 4(c) shows the experimental polarized OAS of AFI-Te (c1) and MOR-Te (c2). Strong Te chain absorption contributes only to the $E//c$ OAS while the much weaker Te ring absorption nearly equally contributes to both $E//c$ and $E \perp c$ spectra ($E//a$ for AFI-Te and $E//b$ for MOR-Te). The AFI-Te-chain spectrum displays an absorption feature at an energy of $\sim$1.7 eV. Since the calculated PBE-exchange–correlation-functional band gaps[6] are usually underestimated, we conclude that the experimental $\sim$1.7 eV gap is in rather good agreement with the theoretical $\sim$1.53 eV gap obtained with the spin–orbit coupling.

No feature is observed around $\sim$1.7 eV in the MOR-Te OAS (Fig. 4(c1)). This confirms that the AFI-Te-chains, probably, have a structure close to that of the perfect Te-helix while the MOR-Te-chains are shorter and less ordered due to strong interaction with MOR. The observed AFI-Te chain band gap of $\sim$1.7 eV is larger than that of bulk t-Te ($\sim$0.33 eV), which is required for Te to be a successor of Si for extremely scaled NWs for modern electronic devices.[5]

The $\lambda = 785$ nm-excitation-wavelength with the photon energy of $\sim$1.58 eV corresponds to the AFI-Te chain absorption edge (Fig. 4(c1)). Therefore, the RS of AFI-Te at this wavelength are resonant RS associated with the corresponding electron transitions. It would be interesting to compare such RS with the RS obtained at a different excitation wavelength. Fig. 4(d) demonstrates the RS of AFI-Te and MOR-Te, namely their cc-spectra, in a wide spectral range obtained with $\lambda = 785$ nm (d1) and $\lambda = 561$ nm (d2) corresponding to a photon energy of $\sim$2.21 eV. The 1st-order band Raman shift of $\sim$168 cm^{-1} remains unchanged for MOR-Te while it noticeably increases for AFI-Te from $\sim$176 cm^{-1} at $\lambda = 785$ nm to $\sim$180 cm^{-1} at $\lambda = 561$ nm. This effect can be explained by assuming correctness of the BZ formalism for AFI-Te-chains. Indeed, due to the Rashba splitting, the electron transitions at the Te-helix absorption edge are shifted far from the Γ-point, with phonons participating in the 785 nm-resonant RS also being shifted. In contrast, contribution of phonons close to the Γ-point (Fig. 2(c) green branch) is high at $\lambda = 561$ nm, the Raman band frequency increasing. Thus, the excitation-wavelength dependence of the AFI-Te chain RS can be considered as an argument in favour of the Rashba splitting in its electron spectrum although photo-induced phenomena like those recently demonstrated for Te nanosheets using time-resolved reflectance spectroscopy[42] cannot be completely ruled out.

A remarkably good agreement between the experimental 2nd-order RS at $\lambda = 561$ nm and Te helix phonon density of states (DOS) obtained from the phonon dispersions (Fig. 2(c)) is demonstrated in Fig. 4(d2). Indeed, three distinct features are displayed at $\sim$340, $\sim$355 and $\sim$368 cm^{-1}. Their positions suggest that the $\sim$340 cm^{-1} and $\sim$368 cm^{-1} bands originate from the doubled frequencies of the phonons at the Γ-point of

the Te chain BZ (Fig. 2(c) blue and green curves, respectively). The $\sim$355 cm^{-1} band can be attributed to the doubled frequency of the X-point phonon. This confirms that the AFI-Te chains are rather regular and close to a 1D crystal. Similar to Si[43] and Ge,[44] the 2nd-order resonant RS of the Te chain depend on the excitation wavelength.

At the same time, the MOR-Te 2nd-order Raman band shows only a slight enhancement compared to the 1st-order band with no change in frequency with change of λ from 785 nm to 561 nm. As we previously pointed out, MOR-Te chains are shorter and more affected by the zeolite matrix than the AFI-Te chains. Therefore, the wave-vector and BZ-critical-point formalism are not acceptable for the MOR-Te chains.

Conclusions

To summarize, we encapsulated tellurium in 1-D submicron-diameter AFI and MOR channels *via* high-pressure-melt injection. Using polarized RS of MOR-Te and AFI-Te single crystals, we discriminated between Te chain and ring Raman bands. We conclude that Te helical chains formed in AFI are rather long, well ordered and weakly interacting with the zeolite. Good agreement of the observed AFI-Te-chain RS with the calculated Te-helix phonon spectrum confirms this. In contrast, Te-chains formed in the MOR-channels are rather short, less ordered and strongly interacting with the zeolite. A probable reason for this is the smaller channel cross-section compared to AFI and the presence of Na$^+$ and Ca^{2+} cations reducing the effective channel cross-section and enhancing interaction with the confined Te species. Therefore, larger hexagonal AFI channels with no cations inside are preferable for the quite long Te chain formation. Te$_8$ and Te$_6$ rings are found in the AFI and MOR channels, respectively, along with the Te chains. Polarized OAS and the excitation-wavelength-dependent resonant RS of AFI-Te provide more evidence for nearly perfect Te-helix formation and its good correspondence with the predicted electronic band structure including Rashba spin splitting. Thus, we succeeded in the first ever experimental study of the phononic and electronic properties of the single Te helix, which is important for development of advanced 1D materials for electronics and spintronics.

To finalize, we stress certain advantages of zeolites over CNTs for the Te-chain study: (1) chains are aligned in relatively large zeolite single crystals allowing polarized RS/OAS measurements as well as obtaining polarized non-linear optical effects like in ref. 45 and (2) zeolites are optically transparent and display no strong Raman bands in the spectral range of the Te chain.

Conflicts of interest

There are no conflicts of interest to declare.

Acknowledgements

Notes and references

1 P. V. C. Medeiros, S. Marks, J. M. Wynn, A. Vasylenko, Q. M. Ramasse, D. Quigley, J. Sloan and A. J. Morris, Single-atom scale structural selectivity in Te nanowires encapsulated inside ultranarrow, single-walled carbon nanotubes, *ACS Nano*, 2017, **11**, 6178–6185.

2 J. K. Qin, P. Y. Liao, M. Si, S. Gao, G. Qiu, J. Jian, Q. Wang, S. Q. Zhang, S. Huang, A. Charnas, Y. Wang, M. J. Kim, W. Wu, X. Xu, H. Y. Wang, L. Yang, Y. K. Yap and P. D. Ye, Raman Response and Transport Properties of Tellurium Atomic Chains Encapsulated in Nanotubes, *Nat. Electron.*, 2020, **3**, 141–147.

3 H. Ikemoto, T. Fujimori, T. Miyanaga, S. Kato, F. Iesari and K. Urita, Structures of Isolated Tellurium Chains Encapsulated Inside Carbon Nanotube, *J. Phys. Chem. C*, 2020, **124**(47), 26043–26047.

4 H. O. H. Churchill, G. J. Salamo, S.-Q. Yu, T. Hironaka, X. Hu, J. Stacy and I. Shih, Toward Single Atom Chains with Exfoliated Tellurium, *Nanoscale Res. Lett.*, 2017, **12**, 488.

5 A. Kramer, M. L. Van de Put, C. L. Hinkle and W. G. Vandenbeghe, Tellurium as a successor of silicon for extremely scaled nanowires: A first-principle study, *2D Mater. Appl.*, 2020, **4**, 10.

6 J. Han, A. Zhang, M. Chen, W. Gao and Q. Jiang, Giant Rashba splitting in one-dimensional atomic tellurium chains, *Nanoscale*, 2020, **12**, 10277.

7 M. H. Brodsky, J. Gambino, E. Smith Jr. and Y. Yacoby, The Raman Spectrum of Amorphous Tellurium, *Phys. Status Solidi B*, 1972, **52**, 609.

8 P. J. Carrol and J. S. Lannin, The Raman spectra of the amorphous Se films, *Solid State Commun.*, 1981, **40**, 81–84.

9 R. M. Martin, G. Lucovsky and K. Helliwell, Intermolecular bonding and lattice dynamics of Se and Te, *Phys. Rev. B: Solid State*, 1976, **13**, 1383–1395.

10 J. Robertson, A new model for the structure of amorphous selenium, *Philos. Mag.*, 1976, **34**, 13–31.

11 L. S. Agroskin, V. N. Bogomolov, A. I. Gutman, A. I. Zadorozhnii, L. P. Rautian and S. G. Romanov, Optical absorption of quasi-one-dimensional lattice of selenium filaments in the mordenite channels, *JETP Lett.*, 1980, **31**, 583–585.

12 V. N. Bogomolov, S. G. Romanov, S. V. Kholodkevich and L. S. Agroskin, The absorption spectra of single selenium and tellurium chains in dielectric matrix channels, *Solid State Commun.*, 1983, **47**, 181–182.

13 V. N. Bogomolov, V. V. Poborchii, S. V. Kholodkevich and S. I. Shagin, Electronic and vibrational spectra of 10 Å selenium clusters and cluster model of amorphous selenium, *Pis'ma Zh. Eksp. Teor. Fiz.*, 1983, **38**, 439–441; *JETP Lett.*, 1983, **38**, 532–535.

14 V. N. Bogomolov, V. V. Poborchii, S. G. Romanov and S. I. Shagin, Raman spectra of chalcogen chains isolated in zeolite matrixes, *J. Phys. C: Solid State Phys.*, 1985, **18**, L313–L317.

15 K. Tamura, S. Hosokawa, H. Endo, S. Yamasaki and H. Oyanagi, The isolated Se chains in the channels of mordenite crystal, *J. Phys. Soc. Jpn.*, 1986, **55**, 528–533.

16 O. Terasaki, K. Yamazaki, J. M. Thomas, T. Ohsuna, D. Watanabe, J. V. Sanders and J. C. Barry, Isolating of individual chains of selenium by incorporation into channels of a zeolite, *Nature*, 1987, **330**, 58–60.

17 J. B. Parise, J. E. MacDougal, N. Herron, R. Farlee, A. W. Sleight, Y. Wang, T. Bein, K. Moiler and L. M. Moroney, Characterization of Se-loaded molecular sieves: A, X, Y, AlPO₄-5 and mordenite, *Inorg. Chem.*, 1988, **27**, 221–228.

18 V. V. Poborchii, Polarized Raman and optical absorption spectra of the mordenite single crystals containing sulphur, selenium or tellurium confined in the one-dimensional nanochannels, *Chem. Phys. Lett.*, 1996, **251**, 230–234.

19 T. Kodaira, M. S. Ivanova, Y. Kiyozumi, H. Takeo, T. Yamamoto and V. V. Poborchii, Study of polarized absorption spectra of Se chain incorporated into zeolite AFI, *Trans. Mater. Res. Soc. Jpn.*, 1996, **20**, 470–473.

20 Z. K. Tang, M. M. T. Loy, J. Chen and R. Xu, Absorption spectra of Se and HgI₂ chains in channels of AlPO₄-5 single crystals, *Appl. Phys. Lett.*, 1997, **70**, 34–36.

21 V. V. Poborchii, A. V. Kolobov, J. Caro, V. V. Zhuravlev and K. Tanaka, Polarized Raman spectra of selenium species confined in nanochannels of AlPO₄-5 single crystals, *Chem. Phys. Lett.*, 1997, **280**, 17–23.

22 V. V. Poborchii, A. V. Kolobov, H. Oyanagi, S. G. Romanov and K. Tanaka, Structure of selenium incorporated into nanochannels of mordenite: dependence on ion exchange and method of incorporation, *Chem. Phys. Lett.*, 1997, **280**, 10–16.

23 V. V. Poborchii, Oriented Se₆ ring clusters in zeolite single crystals: Polarized Raman microscopy, optical absorption spectra and photo-induced effects, *Microporous Mesoporous Mater.*, 2020, **308**, 110559.

24 V. N. Bogomolov, Liquids in ultrathin channels (Filament and cluster crystals), *Usp. Fiz. Nauk*, 1978, **124**, 171–182.

25 W. M. Meier and D. H. Olson, *Atlas of Zeolite Structure Types*, Butterworth-Heinemann, Stoneham, MA, 3rd edn, 1992.

26 *International Zeolite Association Website*, https://www.iza-structure.org/IZA-SC/ftc_table.php.

27 S.-I. Inoue, N. Koshizaki and T. Kodaira, Formation of Te nanowires in zeolite AFI and their polarized absorption spectra, *Int. J. Mod. Phys. B*, 2005, **19**, 2817–2822.

28 T. Kodaira and T. Ikeda, The selective adsorption of tellurium in the aluminosilicate regions of AFI- and MOR-type microporous crystals, *Dalton Trans.*, 2014, **43**, 13979–13987.

29 P. Ghosh, J. Bhattacharjee and U. V. Waghmare, The Origin of Stability of Helical Structure of Tellurium, *J. Phys. Chem. C*, 2008, **112**, 983–989.

30 V. V. Poborchii, Raman spectra of sulfur, selenium or tellurium clusters confined in nano-cavities of zeolite A, *Solid State Commun.*, 1998, **107**, 513–518.

31 V. V. Poborchii, Raman microprobe polarization measurements as a tool for studying the structure and orientation of molecules and clusters incorporated into cubic zeolites: S_8 and Se_{12} rings in zeolite A, *J. Chem. Phys.*, 2001, **114**, 2707–2717.

32 V. V. Poborchii and A. V. Fokin, Raman and optical absorption spectra of oriented Se8 and Se12 rings formed in zeolites: Dependence on the Se loading density, *Microporous Mesoporous Mater.*, 2022, **338**, 111954.

33 V. N. Bogomolov, V. V. Poborchii and S. V. Kholodkevich, Size effects in the vibrational spectrum of 10-A selenium particles, *Pis'ma Zh. Eksp. Teor. Fiz.*, 1985, **42**, 419–421; *JETP Lett.*, 1985, **42**, 517–520.

34 N. Togashi, K. Sugiyama, J. Yu, S. Qiu and O. Terasaki, Single crystal structure analysis of the Se-incorporated mordenite, coupled with the anomalous X-ray scattering, *Solid State Sci.*, 2011, **13**, 684–690.

35 P. Hassanzadeh, C. Thompson and L. Andrews, Absorption Spectra of Tellurium Clusters in Solid Argon, *J. Phys. Chem.*, 1992, **96**, 8246–8249.

36 C. Heinemann, W. Koch and P.-O. Widmark, The tellurium dimer and its anion, *Mol. Phys.*, 1997, **92**, 463–470.

37 M. Ishtiyak, G. Panigrahi, S. Jana, J. Prakash, A. Mesbah, C. D. Malliakas, S. Lebègue and J. A. Ibers, Modulated Linear Tellurium Chains in Ba_3ScTe_5: Synthesis, Crystal Structure, Optical and Resistivity Studies, and Electronic Structure, *Inorg. Chem.*, 2020, **59**, 2434–2442.

38 V. N. Bogomolov, A. N. Efimov, M. S. Ivanova, V. V. Poborchii and S. G. Romanov, Structure and optical properties of a one-dimensional chain of selenium atoms in a cancrinite channel, *Sov. Phys. Solid State*, 1992, **34**, 916–919.

39 V. V. Poborchii, G.-G. Lindner and M. Sato, Selenium dimers and linear chains in one-dimensional cancrinite nanochannels: Structure, dynamics, and optical properties, *J. Chem. Phys.*, 2002, **116**, 2609–2617.

40 V. V. Poborchii, M. Sato and A. V. Shchukarev, Linear dimerized Se chains in cancrinite nanochannels: X-ray diffraction and photoelectron spectra, *Solid State Commun.*, 1997, **103**, 649–654.

41 V. V. Poborchii, A. V. Kolobov, J. Caro, V. V. Zhuravlev and K. Tanaka, Dynamics of single selenium chains confined in 1-dimensional nanochannels of $AlPO_4$-5: temperature dependencies of the 1st and 2nd order Raman spectra, *Phys. Rev. Lett.*, 1999, **82**, 1955–1958.

42 G. Jnawali, Y. Xiang, S. M. Linser, I. A. Shojaei, R. Wang, G. Qiu, C. Lian, B. M. Wong, W. Wu, P. D. Ye, Y. Leng, H. E. Jackson and L. M. Smith, Ultrafast photoinduced band splitting and carrier dynamics in chiral tellurium nanosheets, *Nat. Commun.*, 2020, **11**, 3991.

43 J. B. Renucci, R. N. Tyte and M. Cardona, Resonant Raman scattering in silicon, *Phys. Rev. B: Solid State*, 1975, **11**, 3885–3895.

44 M. A. Renucci, J. B. Renucci, R. Zeyher and M. Cardona, Second-order Raman scattering in germanium in the vicinity of the E_1 and $E_1+\Delta$ edges, *Phys. Rev. B: Solid State*, 1974, **10**, 4309–4323.

45 J. Caro, F. Marlow and M. Wubbenhorst, Optical Second Harmonic Generation of (Dimethylamino)benzonitrile Molecules Incorporated in the Molecular Sieve $AlP0_4$-5, *Adv. Mater.*, 1994, **6**, 413–416.